

ULRR

Fabrication of large single crystals for platinum# based linear polymers with controlled# release and photoactuator performance

Item Type	Article
Authors	Yu, Qi;Li, Mingmin;Gao, Jia;Xu, Peixin;Chen, Qizhe;Xing, Dong;Yan, Jie;Zaworotko, Michael;Xu, Jun;Chen, Yao;Cheng, Peng;Zgabg, Zhenjie
Citation	Angewandte Chemie International Edition;58 (51), pp. 18634-18640
Publisher	John Wiley & Sons, Inc.
Download date	2026-06-16 05:40:11
Item License	https://creativecommons.org/licenses/by-nc-sa/1.0/
Link to Item	https://hdl.handle.net/10344/8426

Akzeptierter Artikel

Titel: Fabrication of Large Single Crystals for Pt-Based Linear Polymers with Controlled-Release and Photoactuator Performance

Autoren: Qi Yu, Mingmin Li, Jia Gao, Peixin Xu, Qizhe Chen, Dong Xing, Jie Yan, Michael J. Zaworotko, Jun Xu, Yao Chen, Peng Cheng, and Zhenjie Zhang

Dieser Beitrag wurde nach Begutachtung und Überarbeitung sofort als "akzeptierter Artikel" (Accepted Article; AA) publiziert und kann unter Angabe der unten stehenden Digitalobjekt-Identifizierungsnummer (DOI) zitiert werden. Die deutsche Übersetzung wird gemeinsam mit der endgültigen englischen Fassung erscheinen. Die endgültige englische Fassung (Version of Record) wird ehestmöglich nach dem Redigieren und einem Korrekturgang als Early-View-Beitrag erscheinen und kann sich naturgemäß von der AA-Fassung unterscheiden. Leser sollten daher die endgültige Fassung, sobald sie veröffentlicht ist, verwenden. Für die AA-Fassung trägt der Autor die alleinige Verantwortung.

Zitierweise: *Angew. Chem. Int. Ed.* 10.1002/anie.201910749
Angew. Chem. 10.1002/ange.201910749

Link zur VoR: <http://dx.doi.org/10.1002/anie.201910749>
<http://dx.doi.org/10.1002/ange.201910749>

Fabrication of Large Single Crystals for Pt-Based Linear polymers with Controlled-Release and Photoactuator Performance

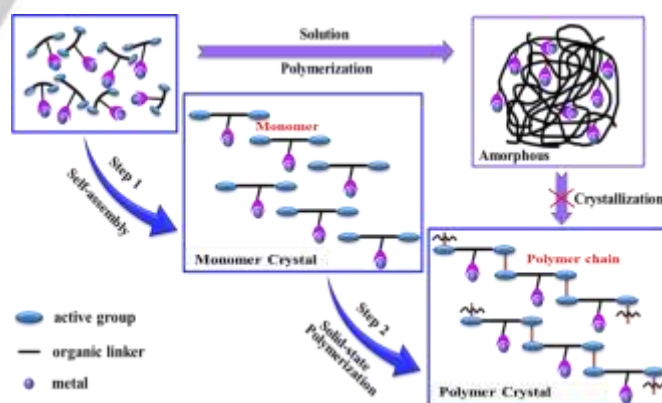
Qi Yu,^{[b],[c],[d]} Mingmin Li,^[a] Jia Gao,^[b] Peixin Xu,^[b] Qizhe Chen,^[b] Dong Xing,^[b] Jie Yan,^[b] Michael J. Zaworotko,^[e] Jun Xu,^[f] Yao Chen,^[a] Peng Cheng^{[b],[d]}, Zhenjie Zhang^{*[a],[b],[d]}

Abstract: Preparation of large single crystals for linear polymers that are amenable to X-ray analysis is very challenging in polymer science. Herein, we employed a coordination driven self-assembly strategy to secure appropriate head-to-tail alignment of anthracene moieties, and for the first time obtained large-sized Pt-based linear polymer crystals through a [4+4] cycloaddition of anthracene in a single-crystal to single-crystal fashion. Using X-ray diffraction analysis to precisely determine polymer crystal structure, we revealed that both the polymerisation and depolymerisation steps proceed via a stable intermediate. Taking advantage of the temperature-dependent slow depolymerization, the afforded Pt-based linear polymer showed potential as a sustained release anticancer drug platform. Furthermore, utilizing the reversible contraction effect of unit-cell volume upon irradiation or heating, the stimuli-responsive crystals were hybridized with polyvinylidene fluoride to obtain a 'smart material' with outstanding photoactuator performance. This work not only provides a new approach to prepare metal-containing linear polymer crystals, but also broadens their potential applications towards drug controlled-release and actuator functions.

Most polymers that are widely applied in our daily life and industry consist of linear structures, e.g. polytetrafluoroethylene (Teflon), polyethylene (PE) and Polyvinylidene fluoride (PVDF).^[1] Polymer performance and properties can be tuned by varying their components and structures. For example, introducing metals (e.g. Pt, Ru) as a new component can endow linear polymers with additional functionalities such as electronic, catalytic, magnetic, bio-sensing, anticancer and radioactivity.^[2] However, varying the structure remains a challenge in polymer science as, in the case of most linear polymers, supramolecular structure remains undefined due to the difficulties involved in obtaining single crystals suitable for single crystal X-ray

diffraction (SCXRD).^[3] Utilizing X-ray techniques, structural details such as molecular packing and interactions may be precisely determined, thereby facilitating a more fundamental understanding of the structure-property relationships involved allowing the development of new functions for linear polymers.

In the past few decades, solid-state topochemical polymerization has attracted considerable interest due to their controllable topological structure and environment-friendly synthesis.^[4] Attributed to the mild solid-state reaction conditions, topochemical polymerization can produce high-quality polymer crystals via a single-crystal to single-crystal (SCSC) transformation which facilitates the determination of polymer single crystal structures via SCXRD.^[5] Moreover, topochemical polymerization has demonstrated potential to produce products that cannot be formed using traditional solution-based methods.^[6] However, the preparation of large crystals for linear polymers using solid-state topochemical reactions is still underexplored. This is largely due to the fact that solid-state polymerisation requires: 1) a well-organized packing mode, 2) a suitably small distance of photoreactive moieties (e.g. C=C bonds require parallel alignment and bond distance $<4.2 \text{ \AA}$),^[7] and 3) an appropriate molecular stacking arrangement (e.g. a head-to-tail manner as shown in Scheme 1). Herein, in order to prepare large crystals of metal-containing linear polymers, we developed a two-step bottom-up synthesis strategy (Scheme 1) involving: (i) coordination-driven self-assembly of monomers to form molecular crystals with appropriate alignment of polymerizable groups; (ii) thereafter producing polymer crystals in a single-crystal to single-crystal manner through topochemical polymerization. This study demonstrates a feasible approach to prepare large crystals for metal-containing linear polymers via topochemical polymerization.



Scheme 1. A stepwise strategy to construct large crystals for metal-containing linear polymers.

Taking advantage of the reversibility of [4+4] cycloaddition reactions and the preferred $\pi \cdots \pi$ stacking manner, anthracene has emerged as one of the most attractive photoreactive groups for topochemical polymerization.^[8] In our previous report,^[9] we found that 1,2-Bis[(anthracen-9-yl)methylene]

- [a] M. Li, Prof. Y. Chen, Prof. Z. Zhang
State Key Laboratory of Medicinal Chemical biology, Nankai University, Tianjin, 300071, China
E-mail: zhangzhenjie@nankai.edu.cn
- [b] Q. Yu, J. Gao, P. Xu, Q. Chen, D. Xing, J. Yan, Prof. P. Cheng, Prof. Z. Zhang
College of Chemistry, Nankai University, Tianjin, 300071, China
- [c] Q. Yu
Shandong Provincial Key Laboratory of Fine Chemicals, School of Chemistry and Pharmaceutical Engineering, Qilu University of Technology, Jinan, 250353, China
- [d] Prof. P. Cheng, Prof. Z. Zhang
Key Laboratory of Advanced Energy Materials Chemistry, Ministry of Education, Nankai University, Tianjin, 300071, China
- [e] Prof. M. Zaworotko
Department of Chemical Sciences, Bernal Institute, University of Limerick, Limerick, V94 T9PX, Republic of Ireland
- [f] Prof. J. Xu
School of Pharmaceutical Science and Technology, Tianjin University, Tianjin, 300071, China

Supporting information for this article is given via a link at the end of the document

Research Articles

WILEY-VCH

amino] ethane (BA2DA) with two photoreactive anthracene blades linked by ethanediamine exhibited a head-to-head packing fashion with an anthracene-anthracene distance of 3.981 Å (Figure 1) which is suitable for [4+4] cycloadditions upon light irradiation. However, due to the inappropriate packing manner, they produced dimer or oligomers instead of ordered linear polymers. The ethanediamine moiety in **BA2DA** is potential to chelate metal cations, thereby breaking the head-to-head packing of **BA2DA** to form a head-to-tail structure resulting from the electrostatic repulsion of metal cations (Figure 1).

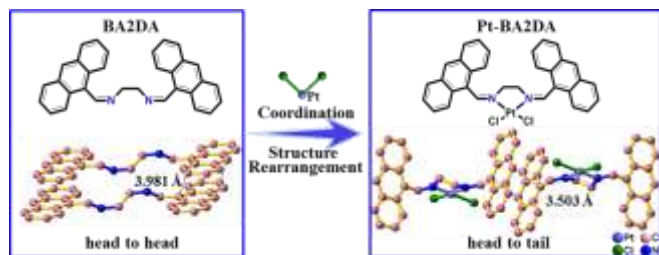


Figure 1. Illustration of the strategy to modify anthracene packing from a head-to-head to a head-to-tail fashion by introducing metal coordination.

To demonstrate the concept to modify the anthracene packing mode, we first introduced Pt(II) ions to coordinate with the **BA2DA** ligand to form a molecular crystal (**Pt-BA2DA**) with a head-to-tail stacking mode (Figure 1).^[10] The reaction of cis-[PtCl₂(DMSO)₂] with **BA2DA** produced yellow plate-like crystals of **Pt-BA2DA** suitable for SCXRD via a slow diffusion method. SCXRD revealed that **Pt-BA2DA** crystallized in the monoclinic space group *C2/c* ($a = 17.06$ Å, $b = 8.19$ Å, $c = 18.90$ Å, $\alpha = \gamma = 90^\circ$, $\beta = 105.6^\circ$, $V = 2545$ Å³). Single crystal structure analysis revealed the Pt(II) ion to be four-coordinated with two N atoms from the **BA2DA** ligand and two chloride ions (Figure 2b and Table S1). As expected, anthracene groups are suitably aligned for topochemical [4+4] cycloaddition. The anthracene blades are aligned in a head-to-tail manner with strong $\pi \cdots \pi$ stacking and anthracene-anthracene distance of 3.503 Å, and the torsion angle of neighboring anthracene groups approaching 0°. UV-Vis spectroscopy revealed that **Pt-BA2DA** showed a broad adsorption peak ranging from 300 to 500 nm. Thus, white light with a wide visible wavelength was chosen to initiate the polymerization reaction in **Pt-BA2DA**. Furthermore, in order to obtain the intact and transparent polymerized crystals, the single crystals of **Pt-BA2DA** were protected in paratone-N oil during irradiation to prevent air oxidation of the 9 and 10 positions of anthracene.^[11]

When the crystals of **Pt-BA2DA** were subjected to irradiation with white light at room temperature for 7 days, a **Pt-BA2DA-i** intermediate was obtained with a low polymerization degree. SCXRD analysis revealed the unit cell of **Pt-BA2DA-i** ($a = 17.60$ Å, $b = 8.08$ Å, $c = 18.33$ Å, $\beta = 106.4^\circ$, $V = 2504$ Å³) showed a contraction (1.6%) of volume while ~44% of anthracene groups were polymerized (Table S2). Further extending the irradiation to longer times did not increase the polymerization degree (~45% after 20 days). Temperature usually plays a key role to the topochemical reaction process. Thereby we attempted lower temperatures such as 265 K to promote the polymerization. We observed a boosted polymerization process: 0 → 44% polymerization degree in 3 days and then to 100% in 7 days. Finally, we obtained high-quality single crystals for **poly(Pt-BA2DA)** with a contracted (3.5%) unit cell ($a = 17.24$ Å, $b = 7.97$ Å, $c = 18.70$ Å, $\beta = 107.3^\circ$, $V = 2455$ Å³) determined via SCXRD

(Figure 2c and Table S3). These results indicated the existence of a two-step photopolymerization process (**Pt-BA2DA** → **Pt-BA2DA-i** → **poly(Pt-BA2DA)**). In the crystal structure of **poly(Pt-BA2DA)**, new C-C bonds with 1.677 Å length were formed between the adjacent anthracene (9, 10-) moieties, that is consistent with the literature results.^[12] We also observed that the polymerization energy was released in the manner of crystal cracking (Figure 2d). We found that the direction of cracks was along (1 0 -1) plane of the crystal, which was corresponding to the polymerization direction (Figure S1). Fortunately, the cracked crystals still possessed large size (~400 μm × 15 μm) and good quality. The distance between adjacent polymer chains is approximately 9.498 Å. The highly ordered alignment and weak intermolecular interactions of linear polymer chains make it possible to exfoliate materials into nanorods.^[13] Adopting a simple mechanical exfoliation method similar to exfoliation of graphene, we are able to harvest well-dispersed nanorods with diameters ~10-20 nm as seen in transition electron microscopy (TEM) images (Figure 2e).

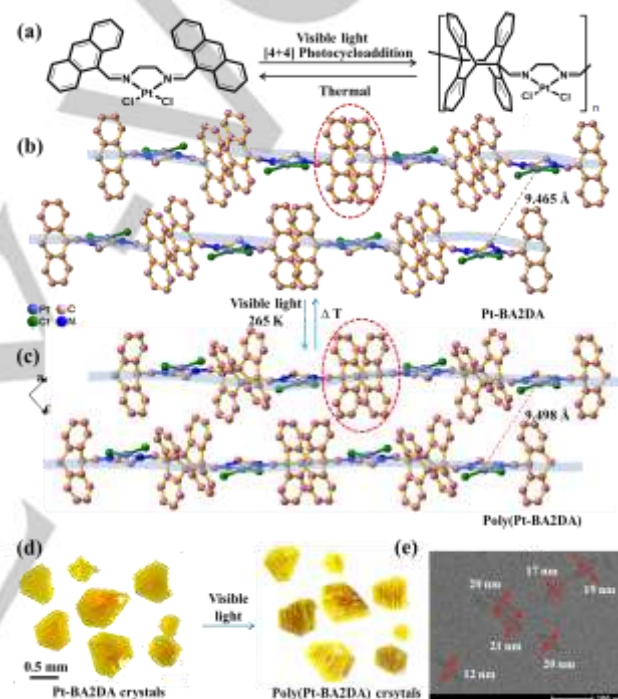


Figure 2. (a) Reversible [4+4] photopolymerization reaction of **Pt-BA2DA**. (b) View of the **Pt-BA2DA** crystal structure along *b* axis. (c) Crystal structure of **poly(Pt-BA2DA)** showing the polymer's connectivity. (d) Optical microscopy images of crystals before and after irradiation illustrating the cracks associated with the topochemical reaction. (e) TEM images of nanorods obtained from **poly(Pt-BA2DA)** after mechanical exfoliation. Color code: C, pink; N, blue; Cl, green; Pt, purple.

In order to study the photoreaction process of **poly(Pt-BA2DA)**, various characterization techniques including powder X-ray diffraction (PXRD), UV-Vis spectroscopy, solid-state ¹³C NMR and FT-IR were employed. Based on an in-house setup (Figure S2), we successfully prepared gram-scale **poly(Pt-BA2DA)** powder. PXRD studies showed that polymerization of **Pt-BA2DA** was completed within 10 days upon light irradiation (44% polymerization degree after 3 days). PXRD patterns of large-scale **Pt-BA2DA**, **Pt-BA2DA-i**(44%) and **poly(Pt-BA2DA)** agreed well with the calculated patterns of single crystal structures, and further confirmed the high purity of the samples

Research Articles

WILEY-VCH

(Figure 3). In addition, this photo-polymerization process can be tracked with sample color change from yellow to light yellow. UV-Vis spectroscopy revealed the absorption band at 445 nm in the visible region, ascribed to π - π^* transition of anthracene, gradually disappear due to the loss of the conjugation after polymerization (Figure S3).^[14]

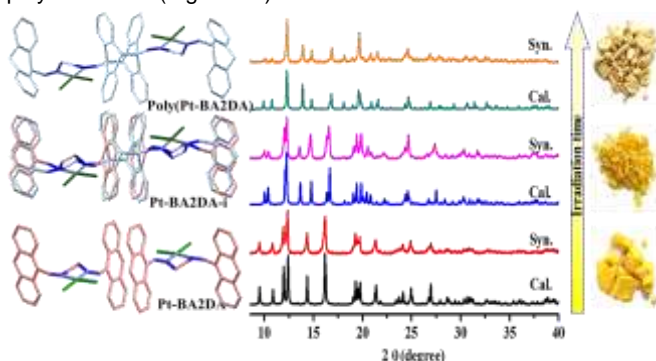


Figure 3. PXRD patterns of **Pt-BA2DA**, **Pt-BA2DA-i** and **poly(Pt-BA2DA)** and their calculated patterns based on single crystal structures. This polymerization process was associated with sample color change.

Solid-state ¹³C NMR and FT-IR was used to further monitor the polymerization process. For the monomer, the primary peaks of aromatic anthracene (ranging 123.9 to 129.0 ppm), with partial overlap, can be attributed to the similar electronic environments within anthracene (Figure S4). Additionally, the carbon peak at 172.5 ppm assigned to -C=N- and the peak at 62.6 ppm assigned to the -CH₂- of the ethanediamine linker can be identified by their standard chemical shifts. After irradiation, a characteristic signal at $\delta = 66.2$ ppm assigned to the bridgehead of dianthracene appeared.^[15] In addition, the polymerization made the two carbons from the ethanediamine linker inequivalent, thereby forming a new peak at 181.0 ppm. Upon extending the reaction time, the -C=N- peak of the monomer at 172.5 ppm gradually vanished. In the FT-IR spectra (Figure S5), the peak at 835 cm⁻¹ ascribed to the medial (e.g. 9, 10-) C-H vibrations in anthracene gradually disappeared as irradiation time extended, while a new peak at 819 cm⁻¹ attributed to the medial C-H bend of dianthracene appeared and its intensity gradually increased.^[8a,13a] All these results revealed that the polymerization of anthracene achieves completion as reaction time is extended.

As reported in literature, the photopolymerization reaction of anthracene is reversible upon thermal treatment. Hence, we studied if **poly(Pt-BA2DA)** can undergo the reverse reaction under thermal treatment. Interestingly, differential scanning calorimetry (DSC) measurement revealed that **poly(Pt-BA2DA)** exhibited two characteristic endothermic peaks attributed to depolymerization: one between 40 °C and 90 °C and the other between 90 °C and 135 °C (Figure 4a and S6). By contrast, the DSC spectra of the intermediate product, **Pt-BA2DA-i**, only exhibited one endothermic peak between 90 °C and 135 °C (Figure 4a), consistent with the second peak observed in **poly(Pt-BA2DA)**. The above results showed clear evidence that depolymerization of **poly(Pt-BA2DA)** proceeds via two processes: first **poly(Pt-BA2DA)** → **Pt-BA2DA-i**, and then **Pt-BA2DA-i** → **Pt-BA2DA**. To the best of our knowledge, such an unprecedented depolymerization with two distinct processes has not been studied in linear polymers as of yet.

In order to further study the depolymerization of **poly(Pt-BA2DA)** in detail, in-situ FTIR, PXRD and SCXRD were

employed to track the depolymerization process of **poly(Pt-BA2DA)** over time. As shown in Figure 4b, **poly(Pt-BA2DA)** gradually depolymerized at 30 °C with the intensity increase of the characteristic peak at 835 cm⁻¹ assigned to the medial C-H (e.g. 9, 10-) of anthracene, eventually reaching a stable intermediate stage after reaction for 24 h. SCXRD revealed that the intermediate structure, with 44% polymerization degree, is very similar to that observed during the reverse polymerization process (Table S4). Upon raising the temperature to 80 °C the characteristic peak at 819 cm⁻¹ attributed to the medial C-H bend of dianthracene completely disappeared, indicating the complete depolymerization of **poly(Pt-BA2DA)** (Figure 4c). ¹H NMR spectroscopy and SCXRD further confirmed the formation of the pure monomer of **Pt-BA2DA** (Figure S7 and Table S5). These results revealed that the stage of depolymerization was closely related to the heating temperatures and indicated that different energy barriers were required for the two depolymerization processes. According to the Beer-Lambert law, the absorbance of a component in a mixture is linearly dependant on its concentration. Therefore, we were able to obtain the reaction kinetics (e.g. Arrhenius parameters) of the depolymerization process via in-situ FT-IR.^[16] When treating **poly(Pt-BA2DA)** at 60 °C, the reaction rate was calculated to be 0.1850 min⁻¹ for **poly(Pt-BA2DA)** → **Pt-BA2DA-i** phase transformation, which is more than two magnitudes higher than that of the **Pt-BA2DA-i** → **Pt-BA2DA** transformation (0.0017 min⁻¹) (Figure 4d and S8). The large difference between the two reaction rates indicates that much higher energy was required for the transformation process of **Pt-BA2DA-i** → **Pt-BA2DA** compared to **poly(Pt-BA2DA)** → **Pt-BA2DA-i** process.^[17] To investigate the different energy requirements for the two distinct depolymerization processes, kinetic studies were then performed. We first studied the **poly(Pt-BA2DA)** → **Pt-BA2DA-i** conversion process at lower temperatures (e.g. 30-40 °C) to avoid the fast transformation of the second depolymerization process (Figure S9), and then raised the treating temperature (e.g. 80-100 °C) to study the second process, **Pt-BA2DA-i** → **Pt-BA2DA** (Figure S10). The conversions at both temperatures steadily increase over time and follows first-order reaction kinetics. The kinetic parameters of different temperatures were summarized in Table S6 and S8. The activation energy of the two depolymerization processes can be calculated by the Arrhenius equation (1). Based on the Arrhenius plot of ln k versus 1/T in Figure 5a and 5b, the activation energy of **poly(Pt-BA2DA)** → **Pt-BA2DA-i** stage and **Pt-BA2DA-i** → **Pt-BA2DA** stage is 79 kJ mol⁻¹ and 108 kJ mol⁻¹, respectively. This result reveals that the reaction pathway from **poly(Pt-BA2DA)** to **Pt-BA2DA-i** needs to climb a lower energy barrier than that of **Pt-BA2DA-i** → **Pt-BA2DA** transformation, which is also supported by our DFT calculations (Figure 5c). This further explains why we always observed a faster transformation from **poly(Pt-BA2DA)** to **Pt-BA2DA-i** than from **Pt-BA2DA-i** to **Pt-BA2DA**.

$$\ln k = \ln A - E_a / RT \quad (1)$$

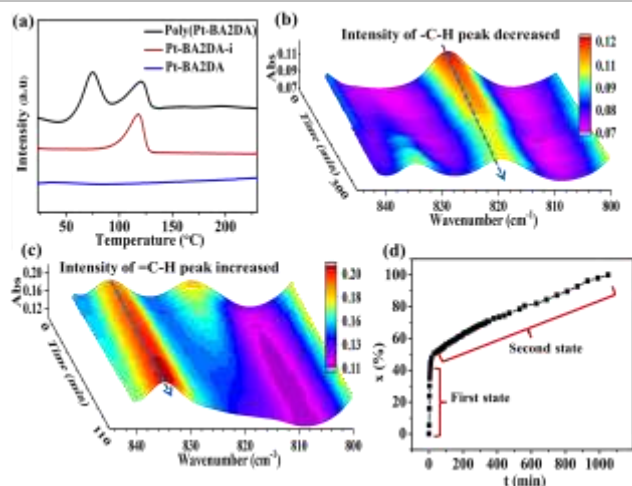


Figure 4. (a) DSC diagram of **poly(Pt-BA2DA)**, **Pt-BA2DA-i** and **Pt-BA2DA**. The spectra changes of (b) **poly(Pt-BA2DA)** at 30 °C and (c) **Pt-BA2DA-i** at 80 °C measured by in-situ FT-IR. (d) Plot of the depolymerization rates of **poly(Pt-BA2DA)** heated at 60 °C.

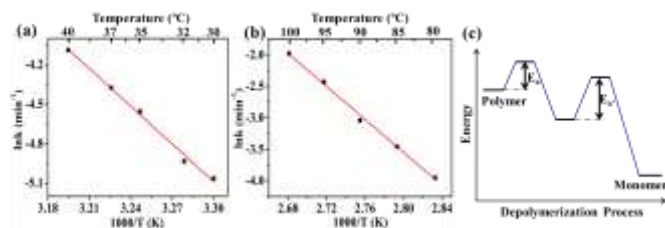


Figure 5. Arrhenius plots of k -values derived from FTIR-temperature-step experiments for **poly(Pt-BA2DA)** at (a) 30–40 °C and for **Pt-BA2DA-i** at (b) 80–100 °C. (c) Activation energy diagram of depolymerization process.

The coordination environment of Pt atoms in **Pt-BA2DA** is similar to that of the Pt-based chemotherapy drugs such as cisplatin which have been widely used as anticancer therapeutic agents.^[18] This structural feature, together with the temperature-dependent depolymerization property, encouraged us to study whether this Pt-based linear polymer could be used as a new type of temperature-dependent controlled-release system to treat diseases such as skin cancer. MTT assay was conducted to evaluate the anticancer properties of **Pt-BA2DA** compared with benchmark cis-platinum toward Skin Cancer A431 Cell lines (Figure S11). The cell viability of both cell lines decreased with the increase of **Pt-BA2DA** concentration. The EC_{50} value for A431 was 5.6 M, which was much better than cis-platinum (30.6 M). For the **poly(Pt-BA2DA)** material, low temperature solubility is poor (i.e. no dissolution observed at 5 °C for 24 h, Figure S12). As the temperature is raised, the amount of dissolved material gradually increased (19%, 34% and 52% for 27 °C, 37 °C and 43 °C, respectively, after 24 h; Figure S13 and Table S8). These results agreed well with the depolymerization results described above. Overall, taking advantage of the temperature-dependent depolymerization property, **poly(Pt-BA2DA)** showed promise as a sustained release system. An in-depth study using **poly(Pt-BA2DA)** as a sustained-release medicine is ongoing in our lab.

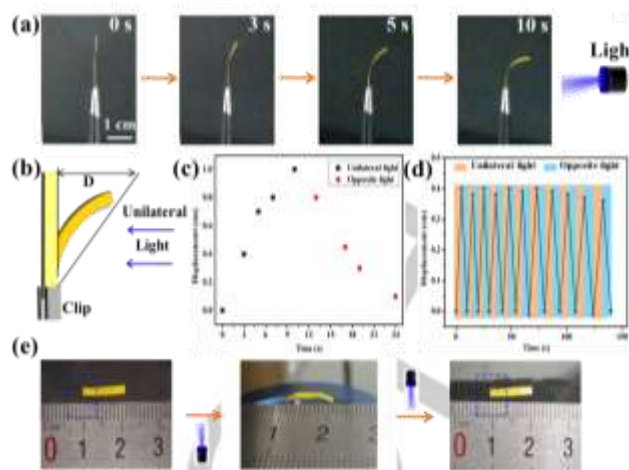


Figure 6. (a) Time-dependent bending towards light of **Pt-BA2DA-PVDF** upon exposure to 440 nm light. (b) Schematic illustration of the defined displacement (D) in the photomechanical process. (c) Plot of displacement against time for the **Pt-BA2DA-PVDF** bending behavior under unilateral light and opposite light. (d) Plot of the repeating cycles of **Pt-BA2DA-PVDF** via changing irradiation direction. (e) Photographs showing that **Pt-BA2DA-PVDF** can crawl via controlling light irradiation.

Photomechanical crystals capable of transforming light energy into mechanical work have attracted wide interests in the fields of photoactuators, soft robotics, optical sensors and smart switches.^[19] Photosalient behavior is typically ascribed to phase transformations accompanied by an anisotropic expansion or contraction of the crystal lattice during a photoreaction upon irradiation, while mechanical motion is induced as strain builds up during the phase transformation. For example, Bardeen *et al.* synthesized plate-like crystals of 9-methylanthracene, which underwent twisting and rolling under irradiation due to the volumetric change of the unit cell.^[20] However, it remains a challenge to use molecular crystals to construct macroscale actuators for practical applications.^[21] Recently, our team created a facile “mixed-matrix membrane (MMM)” approach^[22] which successfully transfers photomechanical crystals (**BA2DA**) with expansion behavior into macroscale photoactuators. These exhibited interesting photoresponsive bending behavior (i.e. bending away from light) due to the nonuniform expansion of crystals upon irradiation. Photoactuators based on photoresponsive crystals are always accompanied by unit-cell change (i.e. expansion or contraction), but most photoresponsive crystals exhibit only expansion behavior. Herein, we reported a rare example of photoactuators constructed based on photoresponsive crystals with contraction behavior under irradiation. In this study, we further developed our MMM approach and successfully fabricated a macroscale actuator, **Pt-BA2DA-PVDF**, by incorporating **Pt-BA2DA** crystals with a contraction effect onto PVDF polymer. PXRD confirmed that **Pt-BA2DA-PVDF** retained the crystallinity of **Pt-BA2DA** (Figure S14). SEM images revealed that a homogeneous membrane was constructed with a thickness of ~25 μm , and **Pt-BA2DA** crystals were uniformly dispersed in the PVDF matrix (Figure S15).

In order to study the photoresponsive properties of **Pt-BA2DA-PVDF**, the membrane was exposed to a 440 nm LED light and the photomechanical deformation was recorded. As predicted, **Pt-BA2DA-PVDF** gradually bent towards incident light direction upon light irradiation (Figure 6a). The bending behavior

could be ascribed to the rapid volume contraction of the membrane side closest to the light source. These results can be further attributed to the photoresponsive **Pt-BA2DA** crystals dispersed in PVDF matrix, which exhibit unit cell contraction effect during photoreaction. We used the defined displacement (D) shown in Figure 6b to measure the degree of the photomechanical property. We found that **Pt-BA2DA-PVDF** quickly bent towards light to reach a displacement of ~1 cm within 10 s. When irradiating from the opposite direction, the **Pt-BA2DA-PVDF** can gradually bend back to the initial position (Figure 6c). This reversible bending process can be repeated through changing the incident light direction (Figure 6d). Moreover, taking advantage the temperature-dependent reversible transformation of anthracene and its photoreaction product, **Pt-BA2DA-PVDF** can easily recover its photoresponsive ability via heating. The reversible bending process can undergo >30 cycles through heating (Figure S16). We found that higher temperature could shorten the recovery time (Figure S17), which is coincident with the depolymerization results mentioned above. We further demonstrated that the **Pt-BA2DA-PVDF** can be used as smart robots to perform various motions. For instance, a robot of **Pt-BA2DA-PVDF** can crawl forward ~1.0 mm after switching the light irradiation direction for only 3 cycles as shown in Figure 6e. These results proved that **Pt-BA2DA-PVDF** offered potential for application as photoactuators and smart robots.

In conclusion, we developed a two-step bottom-up synthesis strategy to produce large single crystals for metal-containing linear polymers involving: (i) coordination-driven self-assembly of monomers to form molecular crystals with appropriate alignment of polymerizable groups; (ii) thereafter producing polymer crystals in a single-crystal to single-crystal manner through topochemical polymerization. We were able to precisely determine the single crystal structure of **poly(Pt-BA2DA)** polymer, and clearly tracked its structural evolution in both the polymerization and depolymerization processes via X-ray diffraction techniques. It was found that both polymerization and depolymerization processed via an intermediate stage (**Pt-BA2DA-i**), and temperature plays a key role in controlling the polymerization kinetics. We further calculated the energy barriers required for the two distinct processes of depolymerization via in-situ FT-IR. This in-depth understanding of the polymerization and depolymerization processes benefits the future design and application of more diverse kinds of polymer crystals. Taking advantage of the temperature-dependent slow depolymerization property of **poly(Pt-BA2DA)** offers high potential to use **poly(Pt-BA2DA)** as platform for the sustained release of medicine. Upon modifying the packing mode of anthracene moieties from head-to-head, to a head-to-tail fashion via metal coordination (**BA2DA** → **Pt-BA2DA**), the photoresponsive behavior of the afforded molecular crystals can be adjusted from 'unit-cell expansion' to 'unit-cell contraction'. Furthermore, the photoresponsive behavior of photoactuators fabricated via hybridization of molecular crystals with PVDF showed adaptable photoresponsive behavior (changing from 'bending away from light' for **BA2DA-PVDF** to 'bending toward light' for **Pt-BA2DA-PVDF**).^[9] Finally, we demonstrated the interesting photoactuator performance of **Pt-BA2DA-PVDF**, such as bending and crawling on the ground. The synthesis strategy reported in this study to prepare large Pt-based polymer crystals is of broad scope, and is likely to be applied to other polymers. Moreover, this study offers new approaches to utilizing linear polymers for advanced applications such as the

controlled release of drugs, actuators and smart robots.

Acknowledgements

The authors acknowledge the National Natural Science Foundation of China (21971126). We thank Prof. W.K. Zhang of Jilin University and Prof. W. Li of Nankai University for DFT calculation and access to measurement facilities. We also thank Yassin H. Andaloussi from University of Limerick for polishing the writing of the manuscript.

Dedication

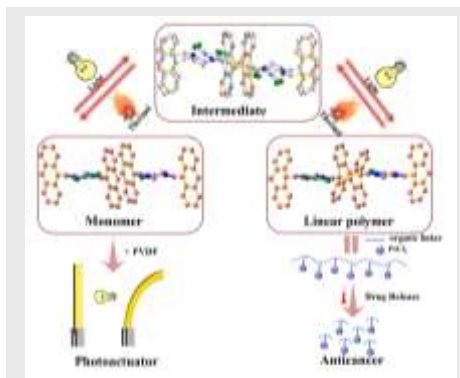
Dedicated to the 100th anniversary of Nankai University

Keywords: Linear polymer • Polymer crystals • Topochemical polymerization • Sustained release • Actuator

- [1] a) L. W. McKeen. *The Effect of Long Term Thermal Exposure on Plastics and Elastomers*, Elsevier Inc, Waltham, **2014**, Ch 1, pp. 1-16. b) J. M. G. Cowie. *Polymers: Chemistry & Physics of Modern Materials*, International Textbooks Comp, Cucks, UK, **1991**, Ch 5.
- [2] a) Y. Yan, J. Zhang, L. Ren, C. Tang, *Chem. Soc. Rev.* **2016**, *45*, 5232-5263. b) K. Kulbaba, I. Manners, *Macromol. Rapid Commun.* **2001**, *22*, 711-724. c) J. B. Heilmann, M. Scheibitz, Y. Quin, A. Sundaraman, *Angew. Chem. Int. Ed.* **2006**, *118*, 934-939. d) W. K. Chan, *Coord. Chem. Rev.* **2007**, *251*, 2104-2118.
- [3] a) Z. Zhang, H. T. H. Nguyen, S. A. Miller, A. M. Ploskonka, J. B. Decoste, S. M. Cohen, *J. Am. Chem. Soc.* **2016**, *138*, 920-925. b) S. Ayala, K. C. Bentz, S. M. Cohen, *Chem. Sci.* **2019**, *10*, 1746-1753.
- [4] a) R. Medishetty, I.-H. Park, S. S. Lee, J. J. Vittal, *Chem. Commun.* **2016**, *52*, 3989-4001. b) Z. Wang, B. Kastern, K. Randazzo, A. Ugrinov, J. Butz, D. W. Seals, M. P. Sibi, Q. R. Chu, *Green Chem.* **2015**, *17*, 4720-4724. c) J. F. Eubank, V. C. Kravtsov, M. Eddaoudi, *J. Am. Chem. Soc.* **2007**, *129*, 5820-5821.
- [5] a) M. Garai, R. Santra, K. Biradha, *Angew. Chem. Int. Ed.* **2013**, *21*, 5548-5551. b) D. Liu, J. P. Lang, B. F. Abrahams, *Chem. Commun.* **2013**, *49*, 2682-2684. c) J. Liu, J. Jia, E. Ruiz, M. Tong, *Chem. Commun.* **2015**, *51*, 15358-15361.
- [6] a) Q. Chu, D. C. Swenson, L. R. MacGillivray, *Angew. Chem. Int. Ed.* **2005**, *117*, 3635-3638. b) G. S. Papaefstathiou, Z. Zhong, L. Geng, L. R. MacGillivray, *J. Am. Chem. Soc.* **2004**, *126*, 9158-9159. c) Y. Han, G. Jin, F. E. Hahn, *J. Am. Chem. Soc.* **2013**, *135*, 9263-9266. d) S. Yang, X. Deng, R. Jin, P. Naumov, M. K. Panda, R. Huang, L. Zheng, B. K. Teo, *J. Am. Chem. Soc.* **2014**, *136*, 558-561.
- [7] G. M. J. Schmidt, *Pure and Applied Chemistry* **1971**, *27*, 647-678.
- [8] a) M. Servalli, N. Trapp, A. D. Schlüter, *Chem. Eur. J.* **2018**, *24*, 15003-15012. b) M. Servalli, M. Solar, N. Trapp, M. Wo, A. D. Schlüter, *Cryst. Growth Des.* **2017**, *17*, 6510-6522.
- [9] Q. Yu, X. Yang, Y. Chen, K. Yu, J. Gao, Z. Liu, P. Cheng, Z. Zhang, B. Aguila, S. Ma, *Angew. Chem. Int. Ed.* **2018**, *57*, 10192-10196.
- [10] J. H. Lee, S. Park, S. Jeoung, H. R. Moon, *CrystEngComm* **2017**, *19*, 3719-3722.
- [11] M. J. Kory, M. Wörle, T. Weber, P. Payamyar, J. Dshemuchadse, N. Trapp, A. D. Schlüter, *Nat. Chem.* **2014**, *6*, 779-784.
- [12] P. Kissel, D. J. Murray, W. J. Wulfstange, V. J. Catalano, B. T. King, *Nat. Chem.* **2014**, *6*, 774-778.
- [13] L. Dou, Y. Zheng, X. Shen, G. Wu, K. Fields, W. Hsu, F. Wudl, *Science* **2014**, *343*, 272-278.
- [14] R. Medishetty, T. T. S. Yap, L. L. Koh, J. J. Vittal, *Chem. Commun.* **2013**, *49*, 9567-9569.
- [15] a) R. Bholra, P. Payamyar, D. J. Murray, B. Kumar, A. J. Teator, M. U. Schmidt, S. M. Hammer, A. D. Schlüter, *J. Am. Chem. Soc.* **2013**, *135*, 14134-14141. b) R. O. Al-Kaysi, R. J. Dillon, J. M. Kaiser, L. J. Mueller, G. Guirado, C. J. Bardeen, *Macromolecules* **2007**, *40*, 9040-9044.
- [16] a) M. C. Rehbein, S. Husmann, C. Lechner, C. Kunick, S. Scholl, *Eur. J.*

- Pharm. Biopharm.* **2018**, *126*, 95–100. b) H. Chen, L. Chang, Y. Jie, *Corros. Sci.* **2017**, *126*, 121–126. c) L. Xiao, F. Li, Y. Li, X. Jia, L. Liu, *RSC Adv.* **2014**, *4*, 41848–41855.
- [17] B. Aguila, Q. Sun, X. Wang, E. O'Rourke, A. M. Al-Enizi, A. Nafady, S. Ma, *Angew. Chem. Int. Ed.* **2018**, *57*, 10107–10111.
- [18] a) L. Feng, M. Gao, D. Tao, Q. Chen, H. Wang, Z. Dong, *Adv. Mater.* **2016**, *26*, 2207–2217. b) R. J. Browning, P. J. T. Reardon, M. Parhizkar, R. B. Pedley, M. Edirisinghe, J. C. Knowles, E. Stride, *ACS Nano.* **2017**, *11*, 8560–8578.
- [19] a) M. Yamada, M. Kondo, J. Mamiya, Y. Yu, M. Kinoshita, C. J. Barrett, T. Ikeda, *Angew. Chem. Int. Ed.* **2008**, *47*, 4986–4988. b) C. Huang, J. Lv, X. Tian, Y. Wang, Y. Yu, J. Liu, *Sci. Rep.* **2015**, *5*, 17414–17422. c) O. M. Wani, H. Zeng, A. Priimagi, *Nat. Commun.* **2017**, *8*, 15546–15553. d) H. Zeng, O. M. Wani, P. Wasylczyk, R. Kaczmarek, A. Priimagi, *Adv. Mater.* **2017**, *29*, 1701814–1701821.
- [20] F. Tong, W. Xu, M. Al-Haidar, D. Kitagawa, R. O. Al-Kaysi, C. J. Bardeen, *Angew. Chem. Int. Ed.* **2018**, *130*, 7198–7202.
- [21] a) T. Lan, W. Chen, *Angew. Chem. Int. Ed.* **2013**, *52*, 6496–6500. b) T. Taniguchi, T. Asahi, H. Koshima, *Crystals* **2019**, *9*, 437–451.
- [22] a) Q. Yu, B. Aguila, J. Gao, P. Xu, Q. Chen, J. Yan, D. Xing, Y. Chen, P. Cheng, Z. Zhang, S. Ma, *Chem. Eur. J.* **2019**, *25*, 1–13. b) Y. Shi, W. Zhang, B. Abrahams, J. Lang, *Angew. Chem. Int. Ed.* **2019**, *58*, 9453–9458.

Herein, we employed a coordination driven self-assembly strategy to secure appropriate head-to-tail alignment of anthracene moieties and for the first time obtained large-sized Pt-based linear polymer crystals through a [4+4] cycloaddition of anthracene in a single-crystal to single-crystal fashion.



Qi Yu, Mingmin Li, Jia Gao, Peixin Xu, Qizhe Chen, Dong Xing, Jie Yan, Michael J. Zaworotko, Jun Xu, Yao Chen, Peng Cheng, Zhenjie Zhang*

Page No. 1– Page No.5

Title: Fabrication of Large Single Crystals for Pt-Based Linear polymers with Controlled-Release and Photoactuator Performance